Proceedings of the IASS Annual Symposium 2016
"Spatial Structures in the 21st Century"
26–30 September, 2016, Tokyo, Japan
K. Kawaguchi, M. Ohsaki, T. Takeuchi (eds.)

Multistable Slit Caps

Paul M. SOBOTA[1], Keith A. SEFFEN[1*]

[1] Advanced Structures Group Laboratory, Department of Engineering, Cambridge University
Trumpington Street, Cambridge CB2 1PZ, UK
[*] kas14@cam.ac.uk

Abstract

Multistable shells are structures that have more than one stable state of self-stress. We demonstrate for the first time that an initially stress-free, hemispherical cap with isotropic behaviour can gain at least three additional stable shapes and, hence, states of self-stress, if it is sliced partially along a given axi-symmetrical meridian. The usual initial and inverted configurations are only slightly affected by slicing. The other configurations are elicited by extra deformations about the inverted shape, which now performs a pre-stressing role. The experimental results are confirmed by finite-element simulations, and it is shown that initially rotationally symmetric structures can gain three stable configurations. Motivated by this, a simplified analytical approach using Föppl-von Kármán plate theory is undertaken to analyse the bistable properties of shallow spherical segments. It is shown that the boundary conditions have a dominating influence on the occurrence of multistability.

Keywords: Bistability, multistability, Föppl-von Kármán plate theory, large deflection shell structures, snap-through buckling, post-buckling analysis, nonlinear varying Gaussian curvature, analytical solution

1. Introduction

Multistable shells are structures that have more than one stable state of self-stress. Applications range from everyday objects, such as flick bracelets and thermostatic switches in kettles, to recent innovations in positional sensors in the field of microelectronics or colour-changing nanomaterials. Modeling these phenomena requires the consideration of geometric non-linearity, and, for the case of shallow shells, Föppl-von Kármán (FvK) plate theory provides an appropriate theoretical framework. Due to the possible application in morphing structures, the topic has gained popularity, again, within the last two decades. Many analytical approaches for bistable shell structures used a uniform curvature (UC) assumption, e.g. Seffen [7], Vidoli and Maurini [11], and Hamouche *et al.* [3], to achieve closed form solutions. Even though UC models violate the out-of-plane Neumann boundary condition (BC) of a vanishing bending moment at a hinged edge, while fulfilling the in-plane BC exactly, the accuracy of these models of the bistable behaviour is relatively good ($\approx \pm 10\%$). With this limiting assumption, shells consisting of isotropic materials are only bistable when they are not pre-stressed [6]. It was shown analytically (Vidoli [11], Hamouche *et al.* [3]) as well as experimentally (Coburn *et al.* [2]) that a third stable state is possible, if orthotropic materials are used or pre-stressing is applied. Recently, more elaborate analytical approaches also considered higher order curvatures: Vidoli [10] demonstrated the increased accuracy of models with up to three degrees of freedom that consider quadratically varying curvature (QVC); other recent approaches demonstrated that non-homogeneous BCs (Brunetti *et al.* [1]) or a non-trivial snap-through process (Seffen and Vidoli [9]) can be captured analytically with higher order models. A specific advantage of these approaches is that the violation of the out-of-plane BCs is at least minimised or completely prevented. The focus of this paper is on the influence of various BCs on multistable behaviour.

In the following section, we demonstrate experimentally tristable shells made from isotropic material, which strongly depend on their boundary conditions. Motivated by these results, a simplified higher order approach is presented in Section 3, which elucidates the influence of different BCs of rotationally symmetric and shallow spherical segments. In Section 4, the results for models with different degrees of freedom are discussed and compared to finite element results. A summary and outlook are given in Section 5.

2. Experiments

2.1. Gaining multistability by slicing

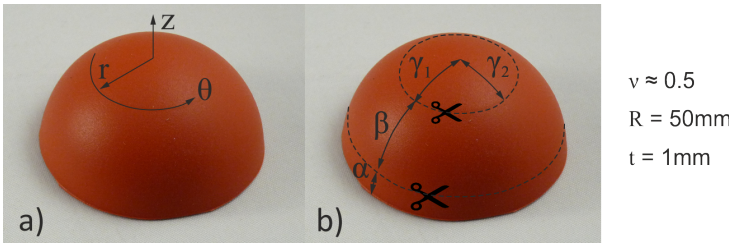

Figure 1: a) Coordinate System; b) Definition of the cutting angles α, γ_1, γ_2 and remaining shell angle β and material properties.

We demonstrate by using isotropic household rubber caps that tristability or higher multistable behaviour is not restricted to orthotropic materials. To understand if the caps were initially stressed due to their manufacturing, samples of the caps were sliced in the radial and circumferential directions. Because no significant extension or compression was observed, the initial form is therefore regarded as stress-free. The description of the geometry and the material properties are depicted in Fig. 1. Different shapes of spherical segments are created by lopping material at the bottom along a meridional length α, as well as the top of the hemisphere. The cut geometry on top is described by the two angles $\gamma_1 \geq \gamma_2$, which define an ellipse when they are projected to the circular planform of the hemisphere. Hence, a slit is described by $\gamma_2 = 0$ and rotational symmetric segments are defined by a circular cutting line with $\gamma_1 = \gamma_2$.

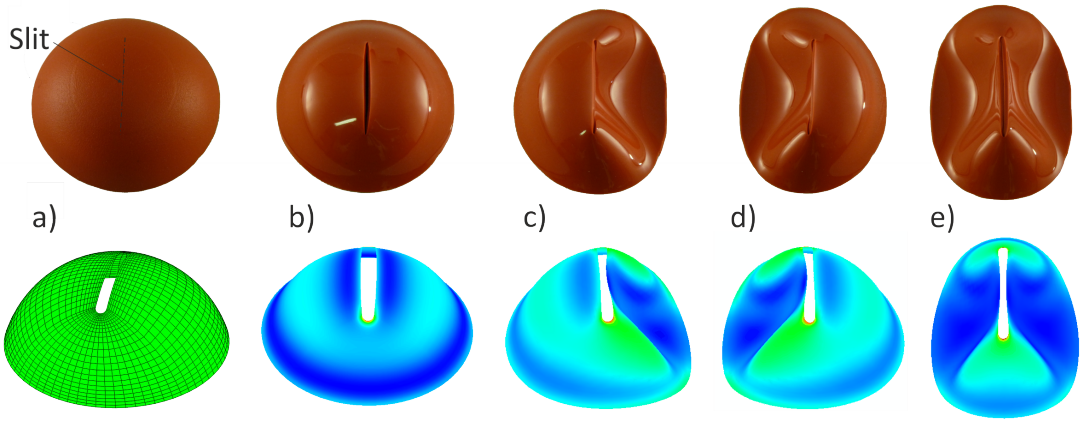

Figure 2: Five stable configurations of a slit cap with $\alpha = 20°$ and $\gamma_1 = 30$: a) initial stress free shape; b) first inverted shape, which is almost axisymmetrical; c) - e): stable perturbations of the first inverted shape. The top row shows the experimental results; the lower part depicts the von Mises stress from finite element (FE) simulations. The width of the slit was set to $\sin(5°) \cdot R$ within the simulations to prevent stress peaks.

Different stable states for segments with $\alpha = 20°$ and a slit of $\gamma_1 = 30°$ are shown in Fig. 2. First the initial configuration (matte surface) was inverted (glossy surface); the additional stable configurations

shown in c) - e) can be triggered independently by applying horizontal forces manually. Three extra configurations are possible and the structure has five stable states in total. Note that applying horizontal forces to the initial configuration causes the shell to snap horizontally, but pop back as soon as the load is removed. To ensure that the experiments are not influenced by imperfections, nonlinear elastic effects, or self-contact of the material in the region near the end of the slit, a finite element simulation with the commercial program ABAQUS [4] was undertaken. Using over 1000 S4 elements in a quasi-static implicit calculation with HHT time integration scheme ($\alpha = 0.05$, Hilber *et al.* [5]) with a Young's modulus $E = 10^7$, density $\rho = 10^{-5}$, Poisson's ratio $\nu = 1/2$ and other parameters as described above, the results are reproduced in Fig. 2. The behaviour is independent of the Young's modulus, but depends on the parameters, $\alpha, \gamma_1, \gamma_2, \nu$ and t, which we have yet to study fully. Nonetheless, from simple physical experiments the influence of the these parameters can be summarised as follows:

- γ_1: for a sliced cap with $\gamma_2 = 0°$ and $\alpha < 40°$, the opening angle γ_1 has to exceed 17°- 19° for $\nu = 0.5$ to cause 'pentastable' behaviour. A further increase of γ_1 leads to inverted shapes that are more likely to stay in this configuration. The configuration similar to 2e) seems preferable because of the self-contact from both sides. Finite element analysis without the consideration of contact shows that a 'reinversion' can occur if the angle exceeds $(90° - \alpha)/2$, where the shell snaps back to its stress-free configuration.
- γ_2 has a diminishing influence on the occurrence of multistability. For geometries in a very small range around $\gamma_1 = \gamma_2 = 40°$ with $\alpha = 0°$ and $\nu = 0.5$, initially rotational symmetric segments are found to show pentastable behaviour.
- The influence of α in the range of $0° \leq \alpha \leq 40°$ on the number of possible stable states is small, whereby a weak negative correlation is observed. When α was further increased, a threshold is reached and shells lose the pentastable behaviour. Interestingly, for $\alpha > 40°$, shells with a long enough slit to cause pentastability, tend to invert nonuniformly in the form of a shallow version of Fig. 2e). Shells that do not show additional stable states for $\alpha < 40°$ are not affected and the inverted shape is approximately uniformly curved.
- Experiments were solely conducted with silicon rubber with the parameters specified in Fig. 1. However, numerical results show that an increasing Poisson's ratio ν strongly favours the occurrence of pentastability.
- As in shallow full plates, a decreasing thickness increases the likelihood of multistability. The influence of the initial radius of curvature is not studied explicitly, since the ratio of R/t is crucial.

Note that it is impossible to rule out the existence of additional states based on finite-element simulations. Even though the loads were carefully adjusted, it is possible that stable states for large γ_1 were missed, because the applied loads led to a reinversion of the shell.

2.2. Spherical Gore

To gain further insight into the perturbed stable configurations, a special case with $\gamma_1 = 90° - \alpha$ is considered, which results in the hemisphere being cut into two symmetrical pieces. These spherical gores are multistable, which is illustrated in Fig. 3a)-d). The first inverted configuration, Fig. 3b), is almost uniformly curved. By rotating the edges, additional stable configurations can be achieved; the structure is metastable for this deformation mode, hence, more stable states were possible than depicted. Even though the shape slightly changes at the sharp edge, the middle of the structure was unaffected. To the authors knowledge, metastability has not been observed for initially stress-free isotropic materials before; and rotating the corners above a critical limit led to a snap-back process. Slicing these gores again along the middle can lead to pentastable shapes, and adding two axisymmetric slices increases the

number even more. The resulting stable configurations are shown in Fig 3 f)-j), whereby the counterparts of the non-symmetric modes g)-i) are not shown. We now introduce an analytical approach to get insight into the structural behaviour, which involves large deflections and bistable behaviour.

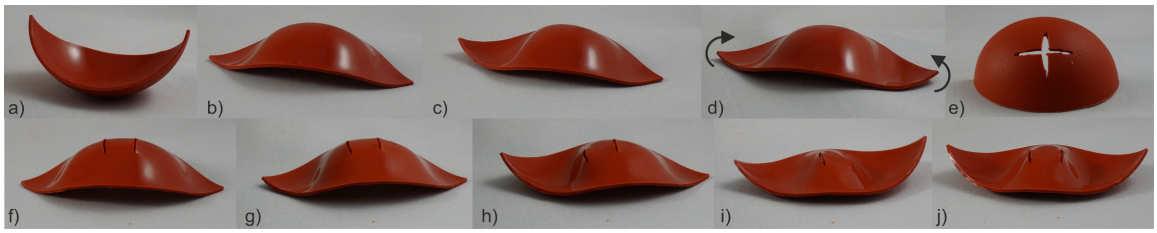

Figure 3: Multiple stable configurations of unsliced (a)-(d) and sliced (e)-(j) spherical gores: a) Stress-free configuration, b) first inverted configuration, c) inverted configuration with a stronger change in curvature at the left corner, d) inverted shape with both edges pointing upwards, where arrows indicate the direction of rotation; e) monostable gore with cross-shaped slice in the middle; f)-j) gores with two parallel slices in circumferential direction: the slit stress-free shape is indistinguishable from a), f) first inverted shape, g) - j) show multiple stable perturbations of f).

3. Analytical approach

Due to the rather small influence of α, it is reasonable to use a shallow shell theory as a first simplification. Even though pentastable behaviour was only observed for non-shallow shells, the inverted shape might give insight into the critical geometry of the slit or hole, respectively. To capture the relatively large deflections, Föppl-von Kármán (FvK) plate theory is applied and adjusted for shells with initial curvature. Because these equations are usually difficult to solve, the following approach is limited to rotational symmetry ($\gamma_1 = \gamma_2$), which simplifies the coupled system of partial differential equations to a problem of coupled ordinary differential equations in cylindrical coordinates r, θ, z. The cases of annular and full plates can then be analysed by solely describing the mid-surface Ω with a constant thickness t, which is bounded by the outer and inner radius a and b, respectively; for the limit of $b \to 0$ a full plate is described. The aim of the analysis is to investigate the correlation between α and γ_1, whereby the first parameter has to be close to 90° to ensure that shallow shell assumption holds for the radial curvature $\kappa_r \ll 1/t$ and slope $dw/dr \ll 1$. An overview of the undertaken Rayleigh Ritz approach, which expands the concept of Seffen and McMahon [8], is given in Fig. 4. By assuming a polynomial expression for the radial curvatures with n degrees of freedom (DOF), the bending energy is expressed solely in terms of this function. Via Gauss's Theorema Egregium, the coupling between the out-of-plane problem in terms of deflection to the in-plane problem, which depends solely on the Airy stress function Φ, is established. As a consequence, Φ can be expressed with respect to the degrees of freedom of the deflected curvatures. The in-plane boundary conditions are satisfied by the constants that arise by solving the differential equation. Firstly, the methodology to achieve the homogenous solution is provided and subsequently the particular solution is elucidated, which is needed for considering various support conditions.

3.1. Homogeneous solution

For large deflections we must consider the effect of the deflection w as well as in-plane displacement u on the mid-plane radial strain: $\varepsilon_r = \partial u_r/\partial r + \frac{1}{2}(\partial w/\partial r)^2$, where the indices r and θ refer to the radial and circumferential direction, respectively; because the influence of large in-plane displacements $(\partial u/\partial r)^2/2$ is however neglected, the theory is restricted to small rotations. Based on this assumption the FvK equations have the form

$$D\nabla^4 w - \frac{t}{r}\frac{\partial}{\partial r}\left[\frac{\partial w}{\partial r}\frac{\partial \Phi}{\partial r}\right] = 0 \qquad \text{(1a)} \qquad\qquad \frac{\nabla^4 \Phi}{E} + \frac{1}{r}\frac{\partial w}{\partial r}\frac{\partial^2 w}{\partial r^2} = 0\,, \qquad \text{(1b)}$$

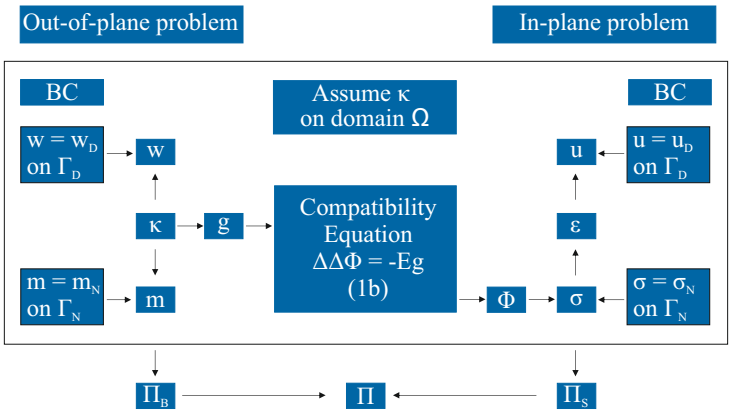

Figure 4: Overview of the coupled nature of the Föppl-von Kármán equations and the Rayleigh-Ritz approach undertaken.

whereby D denotes the flexural rigidity $Et^3/[12(1-\nu^2)]$. These equations can be decoupled into bending- and stretching parts: the first is presented in the following and can be completely described with respect to the out-of-plane deflection w; the latter is provided afterwards and can be characterised by the Airy stress function Φ, which is a potential function of the in-plane stress resultants.

3.1.1. Out-of-plane bending

This is a Rayleigh Ritz approach with n degrees of freedom, denoted by κ_i, where the radial curvatures are assumed to have the form $\kappa_r = \sum_{i=1}^{n} f_i(r)\,\kappa_i$. To address a variety of boundary conditions, it is assumed that each $f_i(r)$ is a polynomial expression with non-negative natural exponents. Hence, the deflection field, w, the circumferential curvatures, κ_θ, and Gaussian curvature, g, are expressed by

$$w = \int\int \kappa_r \,\mathrm{d}r\,\mathrm{d}r \quad , \quad \kappa_\theta = \frac{1}{r}\int \kappa_r \,\mathrm{d}r \quad \text{and} \quad g = \frac{\kappa_r}{r}\int \kappa_r \,\mathrm{d}r\,. \tag{2}$$

The bending stress resultants, m, and shear force, q, are also polynomial expressions. Working with curvatures is equivalent to an assumed deflection, however, by choosing curvature, two constants, B_2 and B_1, that represent a constant deflection and slope, respectively, arise through integration. They are used to satisfy two boundary conditions, which are further discussed in 3.2. For a linear elastic material behaviour the surface integral of the bending energy is solvable analytically:

$$\Pi_B = \frac{1}{2}\int_\Omega \kappa_r m_r + \kappa_\theta m_\theta \,\mathrm{d}A = \pi \int_b^a (\kappa_r m_r + \kappa_\theta m_\theta)\, r\,\mathrm{d}r\,. \tag{3}$$

3.1.2. Mid-plane stretching

Similar to the out-of-plane problem, where the deflection field is a bi-potential function of the curvatures, the in-plane problem can be described by the Airy stress function, Φ. The mid-plane stress resultants are related via $\sigma_r = 1/r\,\partial\Phi/\partial r$ and $\sigma_\theta = \partial^2\Phi/\partial r^2$. Again, assuming a polynomial expression for Φ leads to an analytically solvable integral of the stretching energy

$$\Pi_S = \frac{t}{2}\int_\Omega \varepsilon_r\sigma_r + \varepsilon_\theta\sigma_\theta \,\mathrm{d}A = \pi\, t \int_b^a (\varepsilon_r\sigma_r + \varepsilon_\theta\sigma_\theta)\, r\,\mathrm{d}r\,. \tag{4}$$

To describe the radial displacement, either the relation with the circumferential- or radial strains can be transformed to express

$$u_r = r\,\varepsilon_\theta \qquad \text{or} \qquad u_r = \int \varepsilon_r \,\mathrm{d}r - \frac{1}{2}\int \left(\frac{\mathrm{d}w}{\mathrm{d}r}\right)^2 \mathrm{d}r\,. \tag{5}$$

Note that the first equation is a function of Φ only, while the latter one is a coupled expression.

3.1.3. Solving the coupled problem

To formulate the stretching-bending interaction solely in terms of the previous introduced coordinates, we make use of Gauss's Theorema Egregium

$$g = \kappa_r \kappa_\theta = \frac{1}{r}\frac{\partial \varepsilon_r}{\partial \mathrm{d}r} - \frac{1}{r}\frac{\partial^2(\varepsilon_\theta\, r)}{\partial \mathrm{d}r^2}\,, \tag{6}$$

which establishes a relation between the Gaussian curvature and the mid-plane strains of a surface. For a linear elastic constitutive law the compatibility equation (1b) can be derived, which can be rewritten as

$$-Eg = \frac{\partial^4 \Phi}{\partial r^4} + \frac{2}{r}\frac{\partial^3 \Phi}{\partial r^3} - \frac{1}{r}\frac{\partial}{\partial r}\left[\frac{1}{r}\frac{\partial \Phi}{\partial r}\right]. \tag{7}$$

Denoting the highest order of the polynomial of the deflection w by p, it can be verified that

$$\Phi = \sum_{i=0}^{4p-4} \alpha_i \frac{r^{i+4}}{(i+2)^2(i+4)^2} + \frac{1}{2}C_1 r^2 + C_2 \log(r) + \frac{1}{2}C_3 r^2 \left(\log(r) - \frac{1}{2}\right) \tag{8}$$

satisfies the compatibility equation. Since the Gaussian curvature is a polynomial expression, a corresponding Airy stress function can be found for every coefficient α_i. Quantities that are calculated by only using the first term – the homogeneous solution – are abbreviated by an upper index h. With this relationship, the strain energy function $\Pi = \Pi_B + \Pi_S$ can be expressed with respect to the curvature degrees of freedom. Local minima in this function indicate equilibrium configurations, which are identified via $\nabla\Pi = \mathbf{0}$ and a positive definite Hessian matrix, $\mathbf{H}$, whereby the gradient as well as the Hessian are differentiated with respect to the degrees of freedom κ_i. We determine the constants C_1, C_2 and C_3 in Eqn. (8) next.

3.2. Particular solution

While the homogenous solution can be used for shallow spherical segments in general, in practice we need additional boundary conditions. On a boundary, Γ, these can either be Dirichlet or Neumann BCs that prescribe a displacement/rotation or stress resultants, respectively, which are indicated by the lower index D or N in Fig. 4. Within this paper the cases of a full plate as well as a free edge on the inner side are treated; the outer boundary can be supported by rollers, can be pinned- or clamped. Other cases are straightforward to implement. In mathematical terms, each of these BCs evokes two of the following out-of-plane conditions plus a single in-plane condition:

Clamped Edge:	$w = 0,$	$\partial w/\partial r = 0,$	$u_r = 0\,;$	(9a)
Pinned Edge:	$w = 0,$	$m_r = 0,$	$u_r = 0\,;$	(9b)
Rollers:	$w = 0,$	$m_r = 0,$	$\sigma_r = 0\,;$	(9c)
Free boundary:	$q_r = 0,$	$m_r = 0,$	$\sigma_r = 0\,;$	(9d)
Full plate for $r = 0$:	$q_r = 0,$	$\partial w/\partial r = 0,$	$u_r = 0\,.$	(9e)

3.2.1. Out-of-plane problem

In general a series solution of the form

$$\kappa_r = \sum_{i=0}^{n} \kappa_i r^i \tag{10}$$

can be chosen. Due to integration, the expression for w gains two additional terms $r \cdot B_1 + B_2$. The constant B_2 can be interpreted as an offset of the coordinate system and can be used to satisfy the BC of

$w = 0$ at the outer edge, which does not affect the strain energy stored in the structure. The constant B_1 is equal to the slope at centre of a full plate, hence, it must be zero for $b \to 0$. The shear force is affected by B_1 through the term B_1/r^2 and, therefore, the constant can be determined unambiguously even in the case of a free boundary for $b \neq 0$ and a hinged outer edge. Because there are four out-of-plane BCs in general, the remaining two conditions are fulfilled by reducing the number of degrees of freedom by two. For the case of a full plate, considering only even terms satisfies the BC for the shear force and therefore only one degree of freedom was condensed in these models. For instance, the case of a shell that is clamped at the outer boundary a can be treated by using

$$w = \sum_{i=1}^{n} \left[1 - \left(\frac{r}{a}\right)^2\right]^{i+1} \kappa_i \quad \text{or equivalently} \quad \kappa_r = \sum_{i=1}^{n} 2(1+i) \left[1 - \left(\frac{r}{a}\right)^2\right]^{i-1} \left[(1+2i)\left(\frac{r}{a}\right)^2 - 1\right] \kappa_i \,. \tag{11}$$

This improves the recent approach of Zhang in [12] by introducing additional degrees of freedom, which increases accuracy of the solution. In contrast to various approaches in literature for this extensively discussed problem (see also Zhang [12] for a summary), all BCs as well as the compatibility equations are satisfied.

3.2.2. Satisfying the mid-plane boundary conditions

While consideration of the out-of-plane BCs is straightforward, a further reduction of degrees of freedom to satisfy in-plane BCs would lead to multivalued solutions because the DOF appear as squared terms within the in-plane problem. This is avoided by using the constants C_1, C_2 and C_3 from Eqn. 8. The stress resultants for the derived Airy stress function read

$$\begin{aligned} \sigma_r &= \sum_{i=0}^{4p-4} \frac{\alpha_i r^{i+2}}{(i+2)^2(i+4)} + C_1 + \frac{C_2}{r^2} + C_3 \log(r) \\ \text{and} \quad \sigma_\theta &= \sum_{i=0}^{4p-4} \frac{\alpha_i (i+3) r^{i+2}}{(i+2)^2(i+4)} + C_1 - \frac{C_2}{r^2} + C_3 \left(\log(r) + 1\right) . \end{aligned} \tag{12}$$

For a full plate C_2 and C_3 must be zero to prevent infinite stresses at the centre. Thus, the remaining constant becomes $C_1 = -\sigma_r^h\big|_{r=a}$ or $C_1 = -u_r^h\big|_{r=a}$ in the case of a roller supported or pinned outer boundary, respectively. Since $\sigma_r = \sigma_\theta$ holds for $r = 0$ in this case, the zero displacement condition in the centre is satisfied automatically. Thus, all constants are determined and the boundary conditions are satisfied exactly.

In the case of an annulus C_2 and C_3 can be different from zero. Besides the two in-plane boundary conditions, a third equation is needed for an unambiguous determination of the constants. Since two formulations for the radial displacement exist in Eqn. (5), these equations must be equal to prevent a self-contradicting behaviour. Independently of C_1 and C_2, the latter conditions leads to $C_3 = B_1^2/4$. With this, the remaining constants are straightforward to determine according to the conditions in Eqn. (9). For instance, an outer boundary on rollers leads to

$$C_1 = \frac{a^2 b^2 \left(\frac{B_1^2}{4} \log\left(\frac{a}{b}\right) - \sigma_r^h\big|_{r=a} + \sigma_r^h\big|_{r=b}\right)}{a^2 - b^2} \,, \; C_2 = \frac{B_1^2 \left(b^2 \log(b) - a^2 \log(a)\right) + 4a^2 \sigma_r^h\big|_{r=a} - 4b^2 \sigma_r^h\big|_{r=b}}{4\left(a^2 - b^2\right)} \,. \tag{13}$$

3.3. Extension for initially curved shells

So far the theory was concerned only with initially flat plates, hence, the current configuration denoted by, say, w_c, is identical to the *change* in deflection. To incorporate an initial curvature, an initial deflection w_0 is considered: replacing the deflection with $w = w_c - w_0$ in all equations describes the bending problem

with respect to an initial curvature. Since the initial configuration is stress-free, $m_0 = 0$ must hold and is therefore subtracted from the current bending moment. Hence, the change in the bending stress resultants equals the current bending stress resultants. The same holds for the in-plane problem, so that the change in the Airy stress function also describes the current stresses: Φ is calculated with $g = g_c - g_0$ and represents the potential function of the in-plane stresses in the current configuration. Before the suitability of this shell formulation is evaluated in the following section, nondimensional quantities are introduced:

$$\rho = \frac{r}{a}, \qquad \omega = \frac{w}{t}, \qquad k = \kappa \cdot \frac{a^2}{t}, \qquad S = \frac{\sigma a^2}{Et^2}, \qquad M = \frac{m}{E}\frac{a^2}{t^3} \quad \text{and} \quad U = \Pi \frac{a^2}{t^5 E}. \tag{14}$$

4. Results

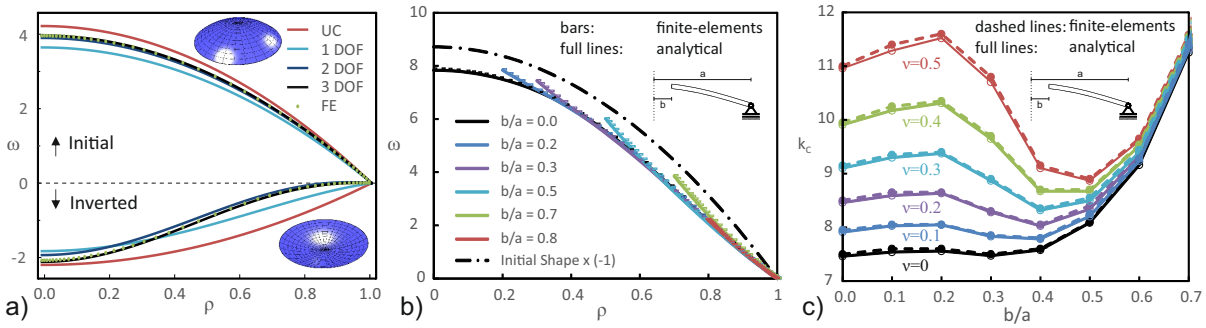

Figure 5: a) Initial critical shape for bistability and corresponding inverted shapes of a full plate with $\nu = 0.1$ for up to three degrees of freedom. b) Inverted configurations of a slit cap with $\alpha = 85°$ over ρ for a/t = 200, $\nu = 0.1$ and 2 DOF. Each line shows the shape for a specific ratio of the inner to outer radius. c) Critical dimensionless curvature k_c for bistability over for a varying hole size b/a for a 3 DOF model with different Poisson's ratios.

The results of the shell formulation are compared to finite element results for various geometries, material properties and boundary conditions. No external load was specified within this Rayleigh-Ritz approach and stable states of self-stress, which are depicted in Fig. 5a) and b) for a deformed full plate and an annulus, respectively, can be calculated. To get an overview of the influence of the hole size, the stable inverted shapes of a cap on rollers with $\alpha = 85°$ are depicted in Fig. 5b) for a 2 DOF model. For shallow shells, the dimensionless curvature is given by $\tan([90° - \alpha]/2)$, which corresponds to $k = 17.46$ for $a/t = 200$. The influence of the size of the hole, given by $R \cdot \sin(\gamma_1) = b$, on the critical curvature for achieving bistability is shown in Fig. 5c) for a 3 DOF approach. In both cases the analytical result coincides very well with the numerical results. For large holes, $b/a > 0.5$, the influence of the Poisson's ratio vanishes and the hole size dominates. As soon as the width of the annulus increases, $b/a < 0.2$, the influence of the Poisson's ratio surpasses the influence of the geometric factor γ_1. Because the constants C_2 and C_3 were only zero for $a/b = 0$, the transition from a full plate to a plate with a tiny hole is not smooth. Due to the inability of a lower order polynomial to capture the rapid change of the radial stresses close to the inner boundary in the latter case, a small discontinuity between the critical curvature of $a/b \to 0$ and $a/b = 0$ arises, which was not observed in finite element simulations. However, using more degrees of freedom, $n > 3$, becomes computationally expensive and solutions for $n > 4$ were not achieved. For these cases, a linearisation of the equations is recommended, which makes it solvable numerically for standard solvers by applying a Newton scheme. As discussed in Section 1, UC models are often applied to predict the bistable behaviour of structures. Because it is sufficient for this purpose to predict the ratio of the stretching to bending energy, a good approximation of the bistable behaviour does not necessarily provide a good approximation of the stress resultants or the deflected

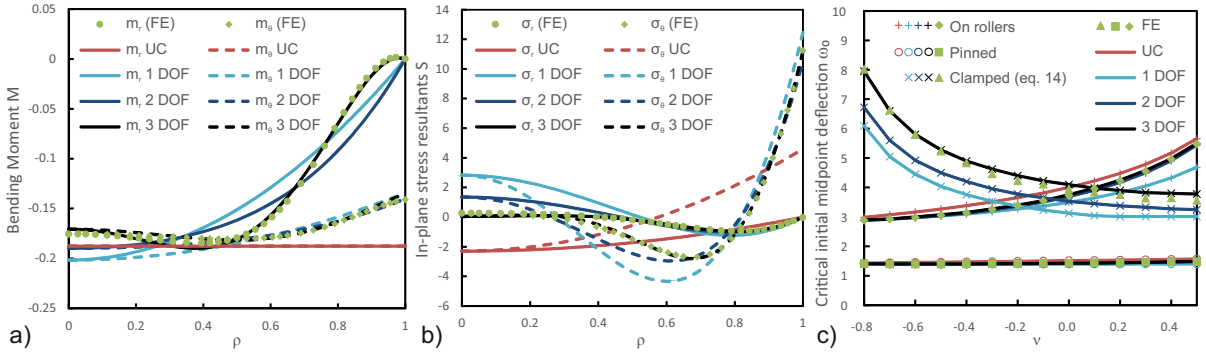

Figure 6: a)/b) Convergence of the bending moments (a) and in-plane stress resultants (b) with increasing number of DOF for a full plate compared to FE results. The bending moments in radial and circumferential direction are identical for the uniform curvature approach; c) Critical initial midpoint deflection to trigger bistability for different boundary conditions and geometries: Boundaries on rollers and pinned edges have uniform initial curvature; for clamped edges the initial configuration is described by Eqn. (11).

shape. To assess the required number of degrees of freedom for both purposes, the out-of-plane and in-plane stress resultants for a shell on rollers are depicted in Fig. 6a)/b) and are compared to the predicted critical shapes in Fig. 6c). The almost indistinguishable, but slightly better, results for a 4 DOF model were not depicted for the sake of clarity. UC models can provide a good estimate of the critical height and curvature, respectively. However, the suitability of the results regarding the stress resultants is not satisfying and therefore, it is recommended that 3 DOF are used (or at least 2 DOF in the case of an annulus) for a better approximation. Nonetheless, omitting 1 DOF leads still to a good approximation of the bistable behaviour. Evaluating the difference between the different cases depicted in 6c) shows, that the influence of the boundary condition is crucial. While a clamped shell that is initially uniformly curved is not bistable at all, bistability becomes possible, as soon as the rotation of the outer edge is no longer restricted. The horizontal supports have a dominating influence and reduce the critical curvature by at least a factor of two. The same holds for the case of an annulus. To avoid a localised problem in the case of a clamped edge, a slightly different case was analysed. The initial shape of the shell is described by Eqn. (11) with $n = 1$. This slight change in geometry leads to a completely different behaviour, and stable states of self-stress become possible for geometries with a critical height that has the same order of magnitude as the non-clamped case; it should be noted that the results for 1 DOF models have been captured in closed form. Seffen showed in [8] that a UC circular shallow shell on rollers needs to exceed an initial midpoint deflection of $\omega_0^2 \geq \frac{16}{1-\nu}$ to show bistable behaviour; adding horizontal supports to the outer boundary changes this value to $\omega_0^2 \geq \frac{16}{7-\nu}$. The threshold for the depicted clamped edge scenario is $\omega_0^2 \geq 14/(23 + 14\nu - 9\nu^2)$.

To demonstrate the suitability of the model of the annulus, the stress resultants for various b/a ratios in the inverted configuration are assessed in Fig. 7. The results for the three DOF model are almost identical to the FE results. A deterioration was observed for $b/a < 0.2$, when the sudden change of the radial stress resultants at the inner boundary cannot be properly represented by a 5th order polynomial expression. However, the estimate of the critical initial geometry provides still a good approximation.

5. Summary

It was demonstrated in experiments that initially stress-free uniformly curved isotropic shells can have five stable configurations, where the boundary conditions have a dominating influence on multistable behaviour. This was shown by partially slicing a shell so that the number of stable states could be either increased or decreased. A simplified analytical Föppl-von Kármán model, which considers various boundary conditions, was presented and the effects on the bistable behaviour were demonstrated. By

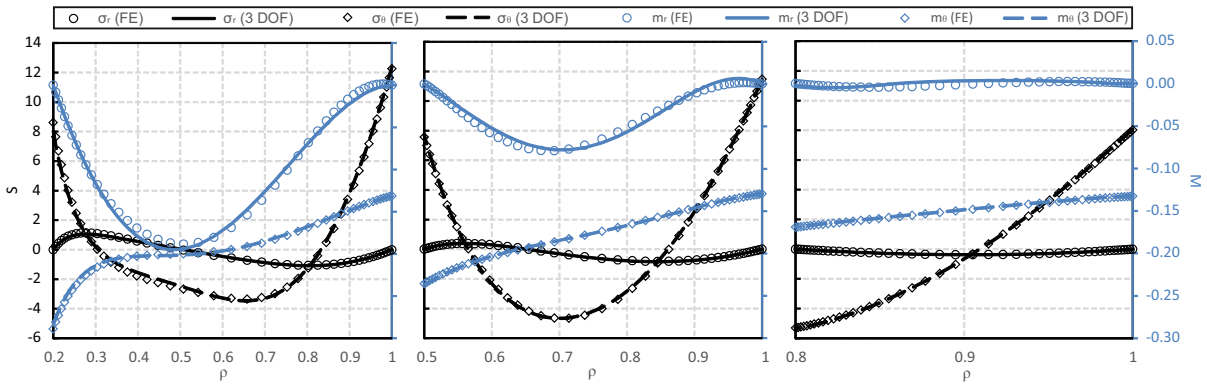

Figure 7: Comparison of analytical model with FEA: Stress resultants for inverted annuli ($\alpha = 85°$, $a/t = 200, \nu = 0.1$) with different ratios of inner/outer radius b/a = 0.2 (left), 0.5 (middle), 0.8 (right); the left axis refers to in-plane stress resultants (black); the right axis to bending moments (blue)

incorporating higher order terms up to four degrees of freedom, the model overcomes the drawbacks of uniform curvature approaches, which are neither suitable for annuli nor for the calculation of the stress resultants. While the bistable properties can be predicted with a lower order model, a good approximation of the stress resultants requires at least two degrees of freedom. Furthermore, the bistable behaviour of structures that have strongly varying Gaussian curvature (e.g. due to clamped edges) can be calculated with higher-order models. Further investigation is necessary to extend the model for non-rotational symmetric modes of deformation.

References

[1] M. Brunetti, A. Vincenti, and S. Vidoli. A class of morphing shell structures satisfying clamped boundary conditions. *International Journal of Solids and Structures*, 2015.

[2] B. H. Coburn, A. Pirrera, P. M. Weaver, and S. Vidoli. Tristability of an orthotropic doubly curved shell. *Composite Structures*, 96:446–454, 2013.

[3] W. Hamouche, C. Maurini, A. Vincenti, and S. Vidoli. Basic criteria to design and produce multistable shells. *Meccanica*, 2016. doi: 10.1007/s11012-016-0375-5.

[4] Hibbitt, Karlsson, and Sorensen. *ABAQUS/standard user's Manual*, volume 1. Hibbitt, Karlsson & Sorensen, 2001.

[5] H. M. Hilber, T. J. Hughes, and R. L. Taylor. Improved numerical dissipation for time integration algorithms in structural dynamics. *Earthquake Engineering & Structural Dynamics*, 5(3):283–292, 1977.

[6] E. G. Loukaides, C. Maurini, and K. A. Seffen. Elementary morphing shells: their complete behaviour. In *Proceedings of the International Association for Shell and Spatial Structures (IASS) Symposium, 21-24 May, Seoul, Korea*, 2012.

[7] K. A. Seffen. Morphing bistable orthotropic elliptical shallow shells. *Proceedings of the Royal Society of London A: Mathematical, Physical and Engineering Sciences*, 463(2077):67–83, 2007.

[8] K. A. Seffen and R. A. McMahon. Heating of a uniform wafer disk. *International Journal of Mechanical Sciences*, 49 (2):230–238, 2007.

[9] K. A. Seffen and S. Vidoli. Eversion of bistable shells under magnetic actuation: a model of nonlinear shapes. *Smart Materials and Structures*, 25(6):065010, 2016.

[10] S. Vidoli. Discrete approximations of the Föppl–von Kármán shell model: from coarse to more refined models. *International Journal of Solids and Structures*, 50(9):1241–1252, 2013.

[11] S. Vidoli and C. Maurini. Tristability of thin orthotropic shells with uniform initial curvature. *Proceedings of the Royal Society of London A: Mathematical, Physical and Engineering Sciences*, 464(2099):2949–2966, 2008.

[12] Y. Zhang. Large deflection of clamped circular plate and accuracy of its approximate analytical solutions. *Science China Physics, Mechanics & Astronomy*, 59(2):1–11, 2016.